

Supporting Information

Graphene Oxide Aptasensor Droplet Assay for Detection of Metabolites Secreted by Single Cells Applied to Synthetic Biology

Dan Zheng¹, Jingyun Zhang¹, Wenxin Jiang², Ying Xu², Haixu Meng²,
Chueh Loo Poh^{1*} and Chia-Hung Chen^{2,3*}

¹Department of Biomedical Engineering, National University of Singapore,
4 Engineering Drive 3, 117583, Singapore

²Department of Biomedical Engineering, City University of Hong Kong,
83 Tat Chee Avenue, Kowloon Tong, Hong Kong, China

³City University of Hong Kong Shenzhen Research Institute,
Shenzhen Virtual University Park, Shenzhen, China

*E-mails: poh.chuehloo@nus.edu.sg; chiachen@cityu.edu.hk

Table of Content

Supporting Information S1 Comparison of the main technologies for single-cell secretion analysis

Supporting Information S2 Droplet microfluidic device

Supporting Information S3 Pico-injector device

Supporting Information S4 The correlation between GO/aptamer ratio and quenching efficiency

Supporting Information S5 The fluorescence recovery at different GO concentrations

Supporting Information-S6 The specificity tests to differentiate ATP and ADP

Supporting Information-S7 ATP droplet GO aptasensor assay

Supporting Information-S8 The pH stability tests of Alexa647-aptamers

Supporting Information-S9 Fluorescence recovery rates to measure naringenins via microplate reader

Supporting Information-S10 The specificity tests to differentiate naringenin, luteolin and apigenin

Supporting Information-S11 The HPLC spectra to measure naringenins in Gib supernatants

Supporting Information-S12 *E. coli* encapsulation rate in the droplets

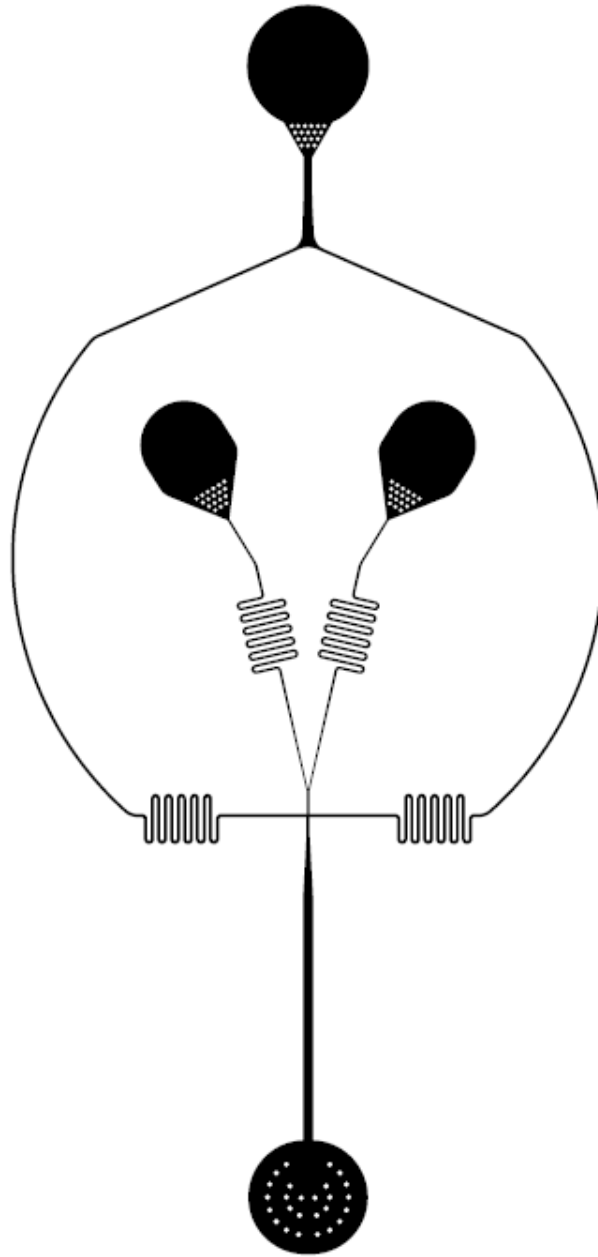
Supporting Information-S13 The relation between pico-injector droplet flow rates and GO aptasensor concentrations in the droplets

Supporting Information-S14 The droplet size change after pico-injection

S1. Comparison of the main technologies for single-cell secretion analysis

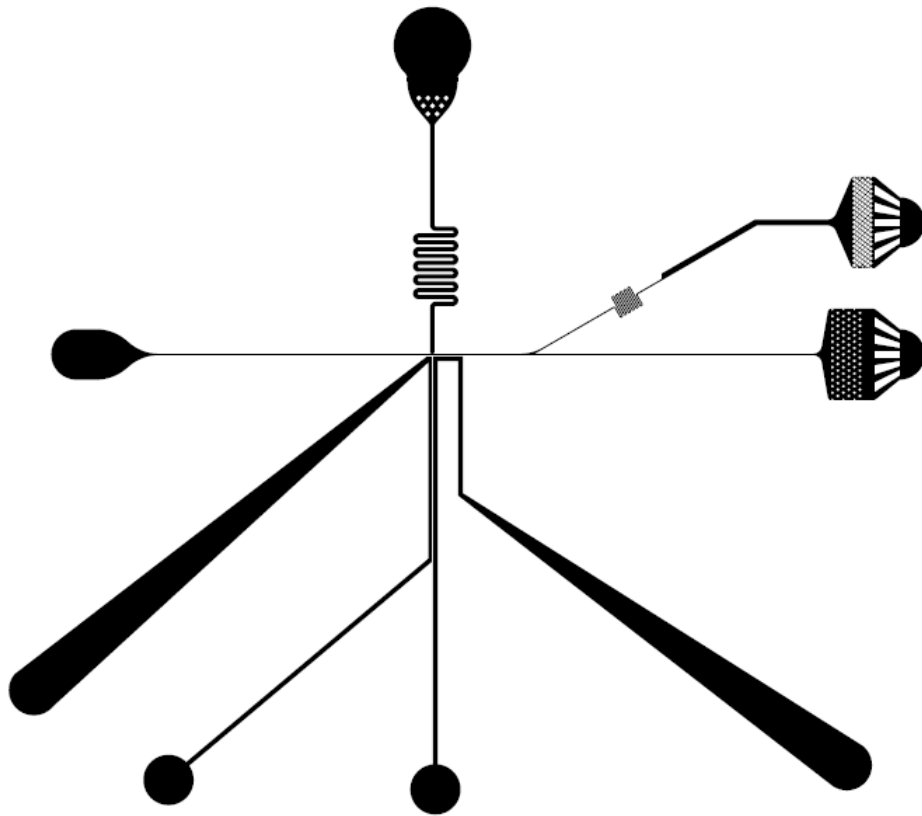
Platform	Flexibility	Sensitivity	Throughput	Target compound
Cell biosensor assay [1,2]	Medium (need to modify cell metabolic circuits)	0.1 mM	High $\sim 10^3$ cells/sec	p-Coumaric acid, D-allulose
Immunosorbent assay on microtiter plates (ELISpot) [3]	High	Spot numbers per experiment	Medium $\sim 10^3$ - 10^4 cells/experiment	Cytokines (IFN- γ , IL-2, TNF- α , etc)
Microwell array with barcode lines [4,5]	High	~ 1 -267 pM	Medium $\sim 10^2$ - 10^3 cells/experiment	Cytokines (IFN- γ , IL-2, TNF- α , etc)
Fluorescence-activated cell sorting (FACS) [6]	Indirect secretion assay	~ 3 μ M	Ultra-high $\sim 10^3$ - 10^4 cells/sec	Trans-cinnamic acid
Mass spectrometry (GC-MS) [7]	High	1.72 nM	Low ~ 1 -cell/experiment	Carbonic anhydrase
High-Performance Liquid Chromatography (HPLC) [8]	High	10.4 nM 56.7 nM 42.4 nM 4.4 nM	Low ~ 1 -cell/experiment	Epinephrine Norepinephrine Dopamine 5-hydroxytryptamine
Droplet enzyme assay [9-12]	Low	~ 1 nM	High $\sim 10^2$ cells/sec	Enzyme activities, intermediate compound, etc.
Droplet RNA-aptamer assay (RAPID) [13]	High	0.3 mM	Ultra-high ($\sim 10^3$ - 10^4 cells/sec)	Tyrosine
Droplet whole cell biosensor [14]	Medium (need to modify cell biosensor)	183.65 μ M	High (~ 100 cells/sec)	Naringenin
This work: Droplet GO aptasensor	High	~ 10 μ M	Ultra-high ($\sim 10^3$ - 10^4 cells/sec)	Naringenin

S2. Droplet microfluidic device.



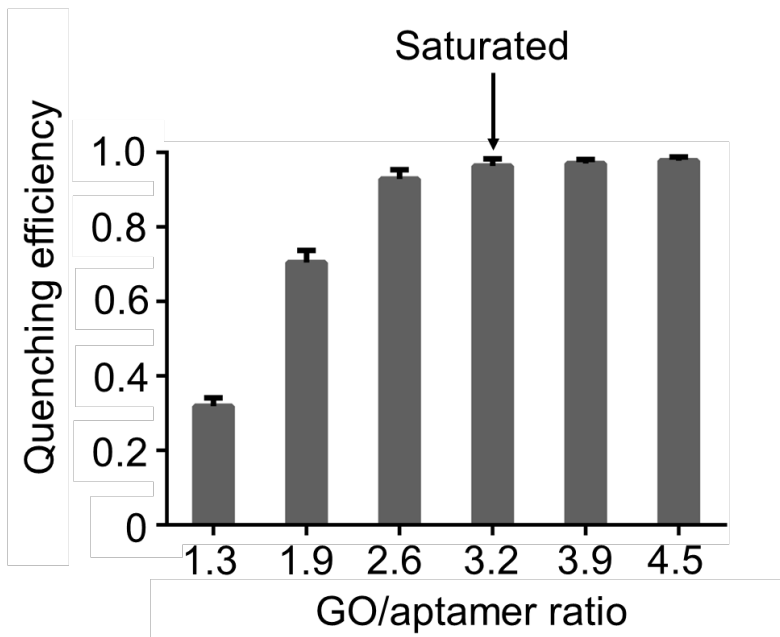
S2. Design of the droplet microfluidic device: The droplet microfluidic device was designed to incorporate a co-flow droplet generator for the encapsulation of individual cells within water-in-oil droplets. The nozzle diameter of the generator was approximately $40\ \mu\text{m}$, ensuring precise control over droplet formation. The microchannel featured a width of $40\ \mu\text{m}$ and a height of $30\ \mu\text{m}$, providing the necessary dimensions for the generation and manipulation of droplets during the experiment.

S3. Pico-injector device



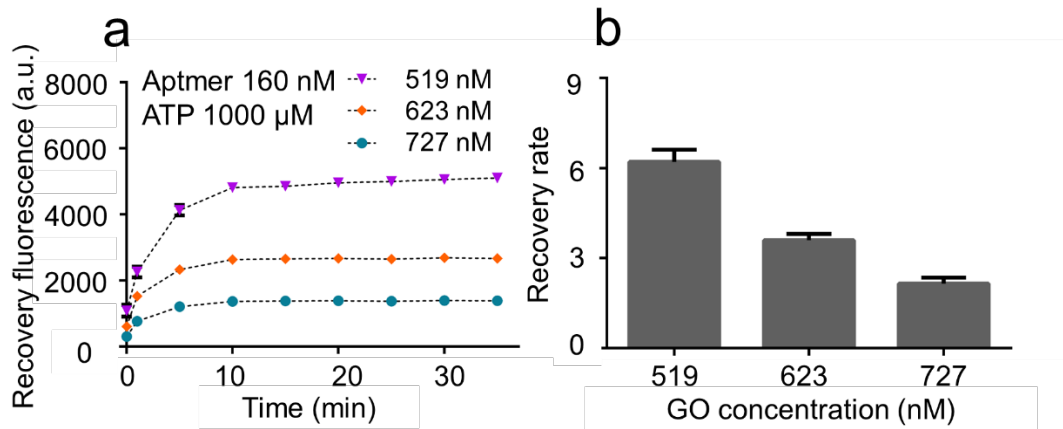
S3. Design of the Pico-injector Device: The pico-injector device was engineered for the precise injection of GO aptasensors into the droplets containing single cells, facilitating the analysis of single-cell secretions. The injector nozzle exhibited a diameter of $20\ \mu\text{m}$, ensuring accuracy in the injection process. The microchannel was designed with a width of $25\ \mu\text{m}$ and a height of $25\ \mu\text{m}$, providing the necessary dimensions for efficient fluid flow and injection of the aptasensors into the droplets.

S4. The correlation between GO/aptamer ratio and quenching efficiency



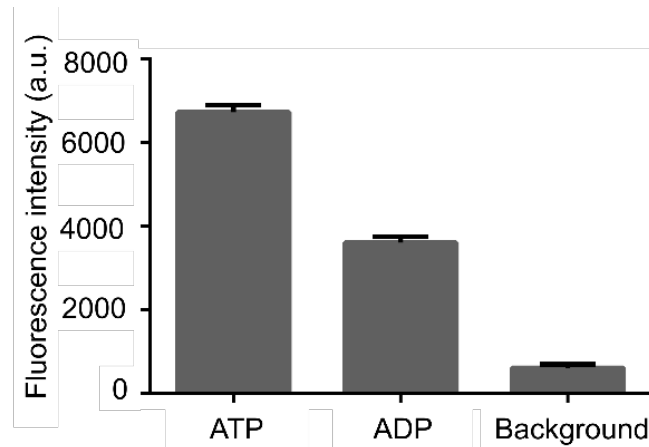
S4. The correlation between GO/aptamer ratio and quenching efficiency is illustrated. It is evident that the quenching efficiency exhibited an upward trend with the escalating GO/aptamer ratio, ranging from 1.3 to 2.6. Subsequently, the quenching efficiency approached saturation levels when the GO/aptamer ratio reached approximately 3.2. Error bars in the figure denote the standard deviation derived from three parallel experiments.

S5. The fluorescence recovery at different GO concentrations



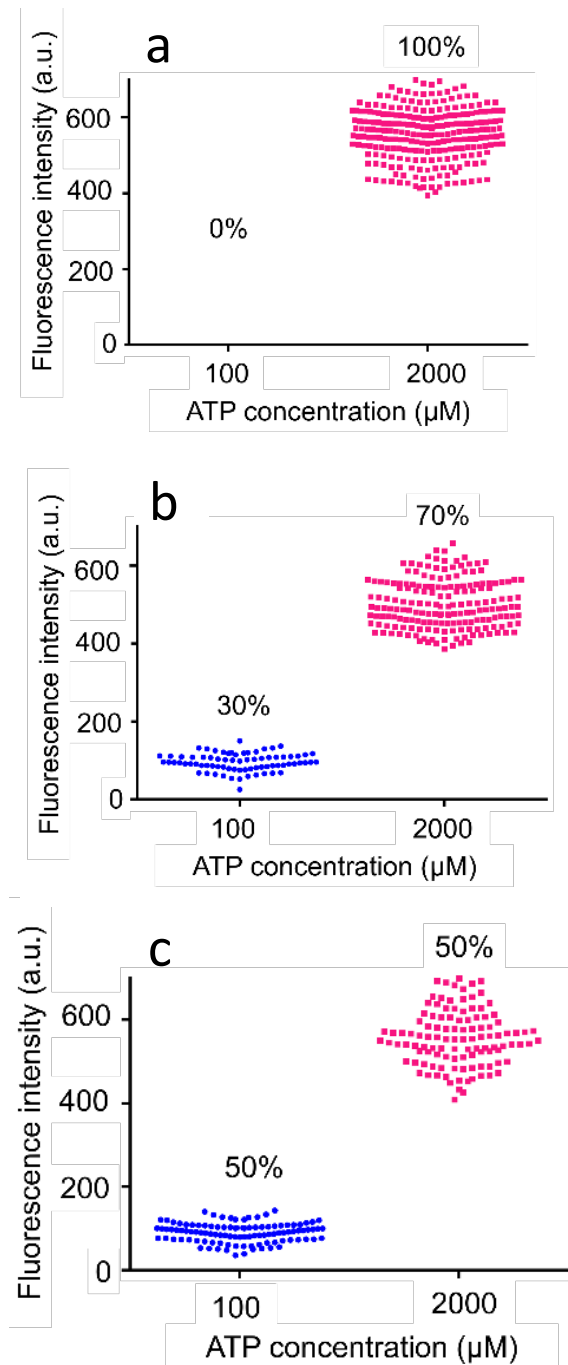
S5. Optimization of GO Concentration: (a) The time-dependent fluorescence recoveries at various GO concentrations were analyzed. The experiments were conducted with a fixed AATP concentration of 160 nM and ATP concentration of 100 μ M. It was observed that the fluorescence recovery intensity increased over time, stabilizing at approximately 20 minutes for all GO concentrations. Notably, within the same incubation period, higher GO concentrations led to a decrease in fluorescence recovery intensity. (b) A correlation analysis between GO concentration and fluorescence recovery rates was performed using the plateau fluorescence signals obtained from the experiments. This analysis provided valuable insights into the relationship between GO concentration and the fluorescence recovery efficiency.

S6. The specificity tests to differentiate ATP and ADP



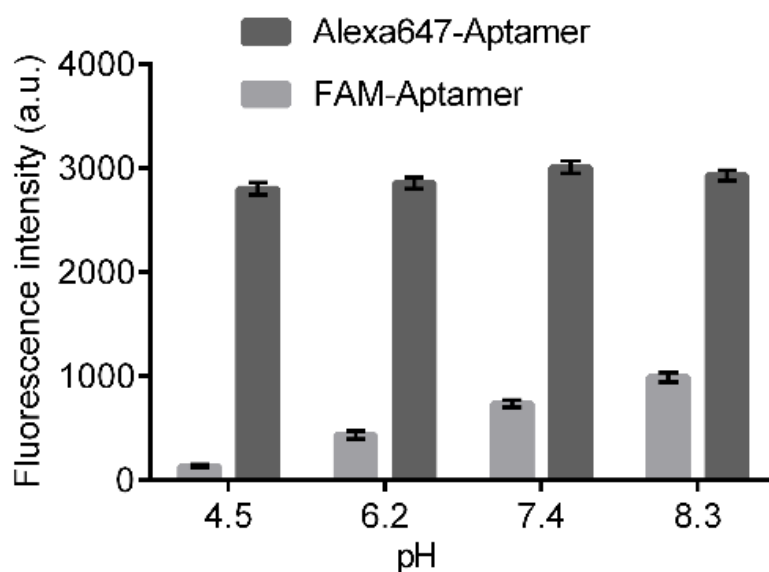
S6. Specificity in Distinguishing ATP and ADP by the ATP GO Aptasensors: The ATP GO aptasensors demonstrated a high specificity in distinguishing between ATP and ADP. When testing ATP at a concentration of 2000 μM , a strong fluorescence signal of approximately 6600 arbitrary units (a.u.) was observed. In contrast, when testing ADP at the same concentration of 2000 μM , the fluorescence signal was significantly weaker, measuring around 3400 a.u. These results highlight the aptasensors' ability to selectively detect ATP over ADP. The standard deviations were calculated based on three parallel experiments to ensure the reliability of the measurements.

S7. ATP droplet GO aptasensor assay



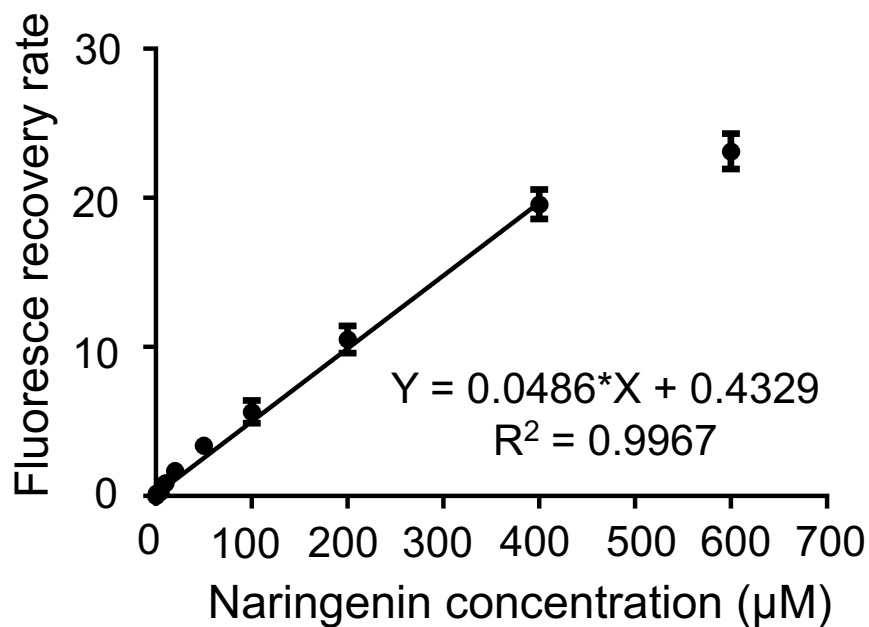
S7. ATP Droplet GO aptasensor assay: The ATP droplet GO aptasensor assay was conducted to assess droplets containing different ratios of ATP concentrations (100 μM and 2000 μM). For each mixing condition (0% : 100%, 30% : 70%, and 50% : 50%), approximately 250 droplets were analyzed. (a) In the case of 0% : 100%, only one distinct droplet population was observed, indicating the absence of low ATP concentration droplets. (b) For the 30% : 70% mixing condition, two separate droplet populations were discerned. Approximately 29.3% of the droplets exhibited low fluorescence intensities, while the remaining 70.7% of the droplets displayed high fluorescence intensities. (c) Similarly, in the case of 50% : 50% mixing, two distinct droplet populations were observed. Around 48.3% of the droplets exhibited low fluorescence intensities, while approximately 51.6% of the droplets displayed high fluorescence intensities. This demonstrates the aptasensor's capability to effectively distinguish between different ATP concentrations within mixed droplets.

S8. The pH stability tests of Alexa647-aptamers



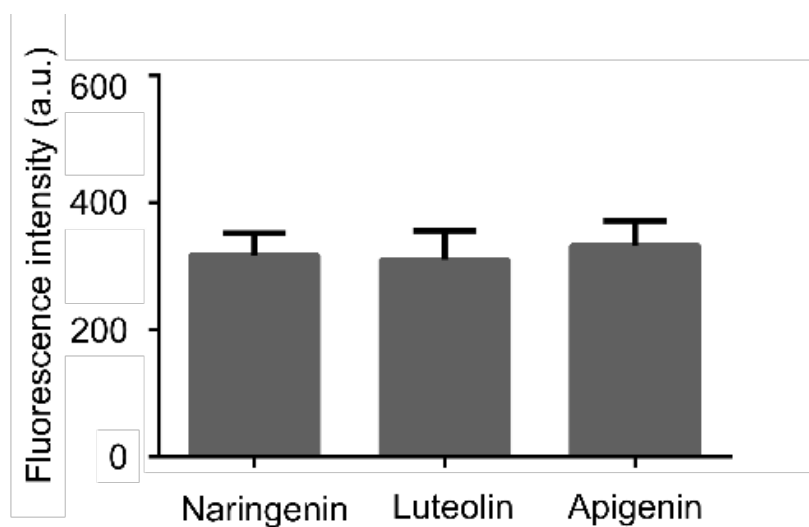
S8. pH Stability Tests of Alexa Fluor 647-Labeled Aptamers and FAM-Labeled Aptamers: The pH stability of both Alexa Fluor 647-labeled and FAM-labeled aptamers was evaluated. As the pH was varied from 4.5 to 8.3, the fluorescence signals of FAM-labeled aptamers exhibited a noticeable change, ranging from approximately 135 a.u. to 992 a.u. In contrast, the fluorescence signals of Alexa Fluor 647-labeled aptamers remained remarkably constant, with an average intensity of about 2900 a.u., indicating high pH stability. Error bars represent the standard deviation of three parallel experiments. This underscores the suitability of Alexa Fluor 647 as a pH-insensitive dye for the GO aptasensor assay.

S9. Fluorescence recovery rates to measure naringenins via microplate reader



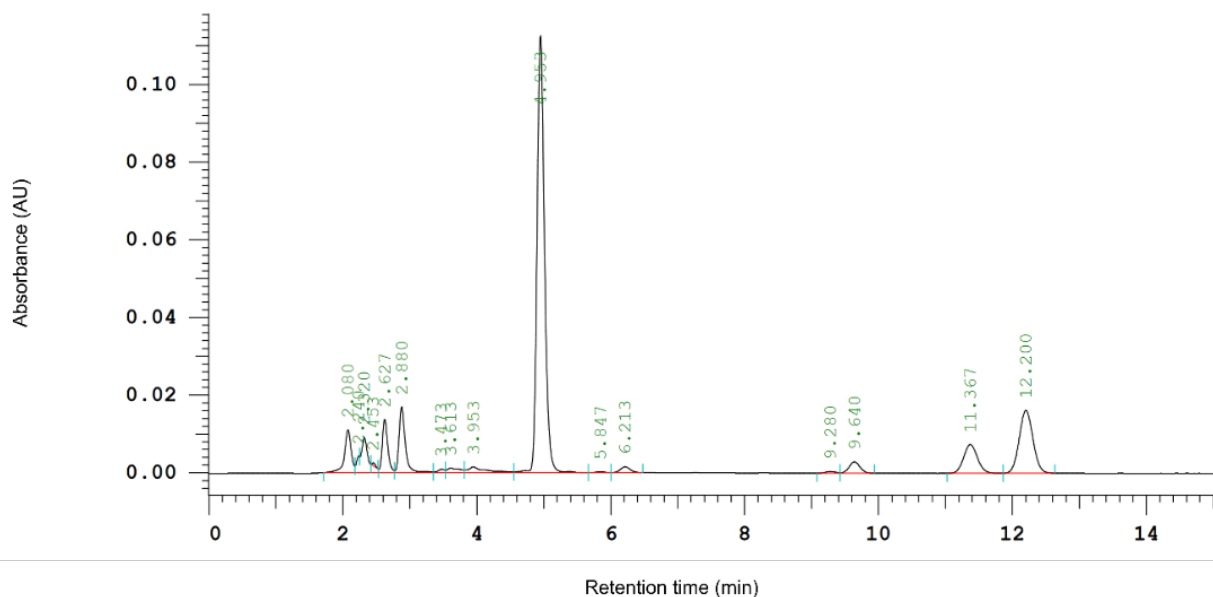
S9. Naringin GO aptasensor characterization: The naringin GO aptasensor was thoroughly characterized using a microplate reader. The results demonstrated a clear linear relationship between naringenin concentrations and fluorescence recovery as the naringenin concentration increased from 0 to 400 µM. At a naringenin concentration of 600 µM, the fluorescence recovery reached an approximate value of ~26. The standard deviations were determined based on data obtained from three independent experiments. This characterization underscores the aptasensor's capability for accurate and reliable naringenin detection over a range of concentrations.

S10. The specificity tests to differentiate naringenin, luteolin and apigenin



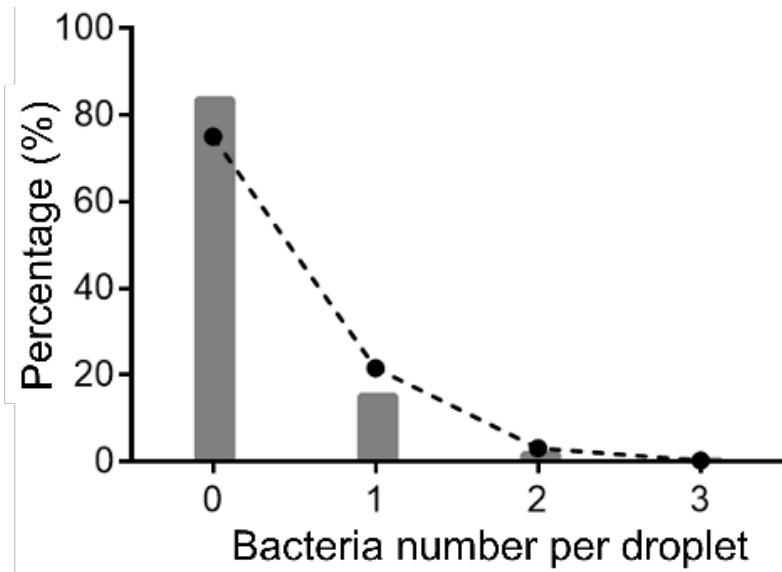
S10. Specificity of GO-Aptasensors: The specificity of GO-aptasensors hinges on the aptamer's capacity to selectively bind to target compounds. This study observed that compounds with similar molecular structures, such as naringenin, luteolin, and apigenin, could not be effectively differentiated using the GO-aptasensors.

S11. The HPLC spectra to measure naringenin in Gib supernatants



S11. HPLC Analysis of Gib Supernatants: To validate the accuracy of the detection results obtained by the droplet GO aptasensors, conventional High-Performance Liquid Chromatography (HPLC) with an absorbance range of 240-500 nm was employed. The HPLC spectra confirmed naringenin concentrations in the Gib supernatant at approximately 104 μM , while no detectable naringenin was found in the WT supernatant. This concurrence between HPLC analysis and aptasensor measurements further attests to the reliability and precision of the droplet GO aptasensor in quantifying naringenin concentrations.

S12. *E. coli* encapsulation rate in the droplets



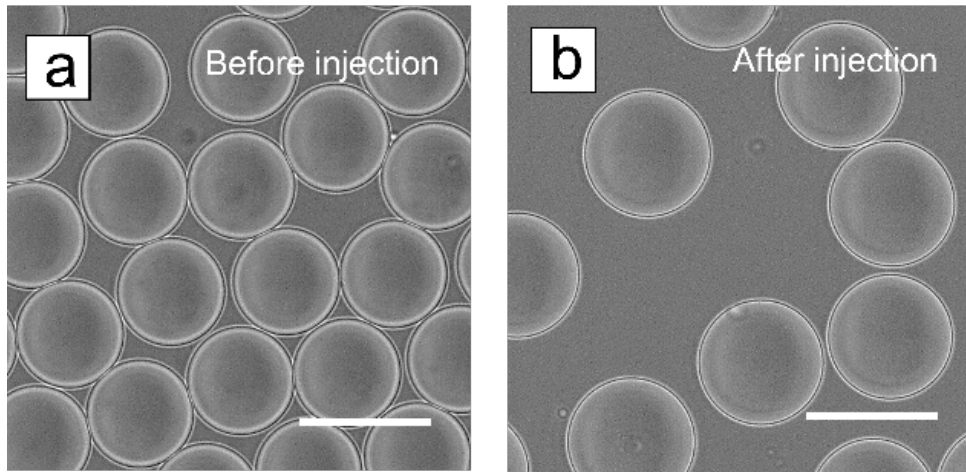
S12. Poisson distribution of *E. coli* encapsulation: The encapsulation of single *E. coli* cells in the droplets followed a Poisson distribution, with an encapsulation rate of approximately 15%. This distribution model provides valuable insights into the statistical nature of the encapsulation process.

S13. The relation between pico-injector droplet flow rates and GO aptasensor concentrations in the droplets

Flow rate of droplet ($\mu\text{L min}^{-1}$)	Droplet diameter before injection (μm)	S.D.	Droplet diameter after injection (μm)	S.D.	Aptamer final concentration in GO-aptasensor after injection (nM)
0.5	39.80	0.09	48.30	0.28	251.13
0.6			47.19	0.14	213.12
0.7			44.83	0.08	160
0.8			43.20	0.12	116.29
0.9			41.31	0.13	56.25

* GO and aptamer concentrations of the GO aptasensors loaded in pico-injector were ~ 1739.7 nM and 533 nM. Flow rates of injector and spacing oil were $0.25 \mu\text{L min}^{-1}$ and $1.2 \mu\text{L min}^{-1}$, respectively. Droplet flow rate was finally set at $0.7 \mu\text{L min}^{-1}$ for the most stable and consistent injections.

S14. The droplet size change after pico-injection



S14. Droplet Size Change after GO Aptasensor Injection: (a) Prior to pico-injection, the droplets had a diameter of $\sim 40 \mu\text{m}$. (b) After pico-injection, the droplet diameter increased to $\sim 45 \mu\text{m}$. This increase in droplet size corresponded to a change in volume.

Reference

1. Solvej Siedler, Narendar K. Khatri, Andrea Zsohár, Inge Kjærboelling, Michael Vogt, Petter Hammar, Christian F. Nielsen, Jan Marienhagen, Morten O. A. Sommer, Haakan N. Joensson. *ACS Synth. Biol.* 2017, 6, 1860-1869.
2. Chao Li, Xin Gao, Hongbin Qi, Wei Zhang, Lei Li, Cancan Wei, Meijing Wei, Xiaoxuan Sun, Shusen Wang, Liyan Wang, Yingbin Ji, Shuhong Mao, Zhangliang Zhu, Masaru Tanokura, Fuping Lu, Hui-Min Qin, *Angew. Chem. Int. Ed.* 2023, 62, e202216721
3. N. Sachdeva, D. Asthana, Cytokine quantitation: technologies and applications, *Frontiers in Bioscience-Landmark*, 2007, 12: 4682-4695.
4. Y. Lu, Q. Xue, M.R. Eisele, E.S. Sulistijo, K. Brower, L. Han, E.D. Amir, et. al., R. Fan, High-throughput secretomic analysis of single cells to assess functional cellular heterogeneity, *Analytical Chemistry*, 2013, 85, 4: 2548-2556.
5. Y. Lu, Q. Xue, M.R. Eisele, E.S. Sulistijo, K. Brower, L. Han, E.D. Amir, et. al., R. Fan, Highly multiplexed profiling of single-cell effector functions reveals deep functional heterogeneity in response to pathogenic ligands, *The Proceedings of the National Academy of Sciences of the United States of America*, 2015, 112(7): E607-E615.
6. L.K. Flachbart, S. Sokolowsky, J. Marienhagen, Displaced by deceivers: prevention of biosensor cross-talk is pivotal for successful biosensor-based high-throughput screening campaigns, *ACS Synthetic Biology*, 2018, 8(8): 1847-1857.
7. Melby JA, Brown KA, Gregorich ZR, Roberts DS, Chapman EA, Ehlers LE, Gao Z, Larson EJ, Jin Y, Lopez JR, Hartung J, Zhu Y, McIlwain SJ, Wang D, Guo W, Diffie GM, Ge Y. High sensitivity top-down proteomics captures single muscle cell heterogeneity in large proteoforms, *Proc Natl Acad Sci U S A.*, 2023, 120(19): e2222081120.
8. V. Carrera, E. Sabater, E. Vilanova, M.A. Sogorb, A simple and rapid HPLC-MS method for the simultaneous determination of epinephrine, norepinephrine, dopamine and 5- hydroxytryptamine: Application to the secretion of bovine chromaffin cell cultures, *Journal of Chromatography B-Analytical Technologies in the Biomedical and Life Sciences*, 2007, 847(2): 88-94.
9. J.J. Agresti, E. Antipov, A.R. Abate, K. Ahn, et. al., D.A. Weitz, Ultrahigh-throughput screening in drop-based microfluidics for directed evolution, *Proceedings of the National Academy of Sciences of the United States of America*, 2010, 107(9): 4004-4009.
10. W.C. DeLoache, Z.N. Russ, L. Narcross, A.M. Gonzales, V.J.J. Martin, J.E. Dueber, An enzyme-coupled biosensor enables (S)-reticuline production in yeast from glucose, *Nature Chemical Biology*, 2015, 11(7): 465-473.
11. T. Beneyton, S. Thomas, A.D. Griffiths, J.M. Nicaud, A. Drevelle, T. Rossignol, Droplet-based microfluidic high-throughput screening of heterologous enzymes secreted by the yeast *Yarrowia lipolytica*, *Microbial Cell Factories*, 2017, 16: 18.
12. J.H. Yang, R. Tu, et. al., L.L. Zhu, Recent advances in droplet microfluidics for enzyme and cell factory engineering, *Critical Reviews in Biotechnology*, 2021, 41(7): 1023-1045.
13. J. Abatamarco, M.F. Sarhan, et. al., A.R. Abate, RNA-aptamers-in-droplets (RAPID) high-throughput screening for secretory phenotypes, *Nature Communications*, 2017, 8: 332.
14. E.K. Bowman, J.M. Wagner, S.-F. Yuan, et. al., H.S. Alper, Sorting for secreted molecule production using a biosensor-in-microdroplet approach, *Proceedings of the National Academy of Sciences of the United States of America*, 2021, 118(36): e2106818118.